Journal of Pharmacological Sciences 137 (2018) 177–186

Contents lists available at ScienceDirect

Journal of Pharmacological Sciences

journal homepage: www.elsevier.com/locate/jphs

Full paper

Simultaneous monitoring of mouse respiratory and cardiac rates through a single precordial electrode

Motoshige Sato [a], Nobuyoshi Matsumoto [a, *], Asako Noguchi [a], Toya Okonogi [a], Takuya Sasaki [a, b], Yuji Ikegaya [a, c]

[a] Graduate School of Pharmaceutical Sciences, The University of Tokyo, Tokyo, 113-0033, Japan
[b] Precursory Research for Embryonic Science and Technology, Japan Science and Technology Agency, 4-1-8 Honcho, Kawaguchi, Saitama, 332-0012, Japan
[c] Center for Information and Neural Networks, National Institute of Information and Communications Technology, Suita City, Osaka, 565-0871, Japan

ARTICLE INFO

Article history:
Received 19 February 2018
Received in revised form
23 May 2018
Accepted 28 May 2018
Available online 20 June 2018

Keywords:
Electrocardiograms
Respiration
Olfactory bulb
Membrane potentials
Local field potentials

ABSTRACT

Normal respiratory and circulatory functions are crucial for survival. However, conventional methods of monitoring respiration, some of which use sensors inserted into the nasal cavity, may interfere with naïve respiratory rates. In this study, we conducted a single-point measurement of electrocardiograms (ECGs) from the pectoral muscles of anesthetized and waking mice and found low-frequency oscillations in the ECG baseline. Using the fast Fourier transform of simultaneously recorded respiratory signals, we demonstrated that the low-frequency oscillations corresponded to respiratory rhythms. Moreover, the baseline oscillations changed in parallel with the respiratory rhythm when the latter was altered by pharmacological manipulation. We also demonstrated that this method could be combined with *in vivo* whole-cell patch-clamp recordings from the hippocampus. Thus, we developed a non-invasive form of respirometry in mice. Our recording method using a simple derivation algorithm is applicable to a variety of physiological and pharmacological experiments, providing an experimental platform in studying the mechanisms underlying the interaction of the central nervous system and the peripheral functions.

1. Introduction

Normal function of the respiratory and circulatory systems is indispensable for survival. Catastrophic failure of either system leads to fatal diseases. Accordingly, electrocardiograms (ECGs) are widely used to quantify cardiac function.[1,2] Likewise, CO_2 sensors and thermally sensitive resistors in the nasal cavity, which detect respiration-related changes in CO_2 concentration and intranasal temperature, respectively,[3,4] are often used to measure respiratory rates. However, these measurements *per se* occasionally affect respiratory rates,[5] making it difficult to obtain intact respiratory information. This matter is particularly the case when small experimental animals are tested. Therefore, more reliable methods are required to measure intact respiratory rhythms.

In humans, a somewhat simple and non-invasive method in which the respiratory rhythms are mathematically isolated from the ECG signal has been clinically applied for monitoring the states of patients with sleep apnea syndrome or evaluating the exercise intensity.[6,7] Although the mathematical algorithm has allowed to derive the respiratory component from human ECGs, it remains unknown whether intact respiratory information can be derived from ECGs of small animals using simple statistical methods.

In the present study, we employed a single-point, direct measurement of ECGs from the pectoral muscles of anesthetized and waking mice. We found periodical slow oscillations in the ECG baseline. The periodic low-frequency (*i.e.*, approximately 3–4 Hz) oscillations reflected a respiratory component, which was assessed by two parameters of respiratory rhythms, *i.e.*, abdominal movement recorded through an isotonic transducer and local field potentials (LFPs) from the olfactory bulb. Moreover, we pharmacologically manipulated the respiratory rhythms of mice to examine whether the ECG low-frequency component changes in parallel with respiratory patterns. Finally, we applied this simple and reliable technique in combination with whole-cell patch-clamp

* Corresponding author. Laboratory of Chemical Pharmacology, Graduate School of Pharmaceutical Sciences, The University of Tokyo, 7-3-1 Hongo, Bunkyo-ku, Tokyo, 113-0033, Japan. Fax: +81 3 5841 4786.
E-mail address: matsumoto.nobuyoshi.0904@gmail.com (N. Matsumoto).
Peer review under responsibility of Japanese Pharmacological Society.

https://doi.org/10.1016/j.jphs.2018.06.009

recordings from hippocampal CA1 neurons and investigated the correlations between respiratory/circulatory functions and the central nervous systems.

2. Materials and methods

2.1. Animal ethics

All animal experiments were performed with the approval of the animal experiment ethics committee at the University of Tokyo (approval numbers: 29-9, 29-12, 29-14 and 29-15) and in accordance with the University of Tokyo guidelines for the care and use of laboratory animals. These experimental protocols were conducted in accordance with the Fundamental Guidelines for the Proper Conduct of Animal Experiments and Related Activities in Academic Research Institutions (Ministry of Education, Culture, Sports, Science and Technology, Notice No. 71 of 2006), the Standards for Breeding and Housing of and Pain Alleviation for Experimental Animals (Ministry of the Environment, Notice No. 88 of 2006) and the Guidelines on the Method of Animal Disposal (Prime Minister's Office, Notice No. 40 of 1995). All animals were housed under a 12-h/12-h dark–light cycle (*i.e.*, lights on from 07:00 to 19:00 for Figs. 1–3, 5; lights off from 07:00 to 19:00 for Fig. 4) at 22 ± 1 °C with *ad libitum* food and water.

2.2. Surgery

For physiological recordings from anesthetized mice, except for whole-cell recordings (*i.e.*, Figs. 1–3), 21- to 39-day-old male ICR mice (Japan SLC, Shizuoka, Japan) were used. The animals were anesthetized with 2.25 g/kg intraperitoneal urethane. Anesthesia was confirmed by the lack of paw withdrawal, whisker movement, and eye blink reflexes. A 1.0-cm incision was made in the precordial skin at a distance of 2.0 mm away from the midline, and a wire electrode (stainless steel wires; AS633, Cooner Wire Company, 15 cm long, 0.147 mm in diameter) was implanted in the pectoral muscle to record the ECG signals. The scalp was removed, and a metal head-holding plate was mounted on the skull. The plate was fixed firmly with dental cement. Then, a hole was made in the back of the head with a drill, and a stainless screw was implanted in the bone above the cerebellum to serve as ground. The screw was attached to a conductive lead wire (UEW, Oyaide Elec, Japan, Tokyo, 15 cm long, 0.14 mm in diameter). Then, a craniotomy was performed using a high-speed drill to create a hole (0.5 mm in diameter) centered at 1.5 mm anterior and 1.0 mm lateral to the bregma, and an electrode was inserted into the olfactory bulb to record LFPs. A suture thread was hooked to the subcutis of the side of the abdomen and was tied to an isotonic transducer, which converted the tension of the thread into electrical potentials.

For chronic recordings of ECG signals and olfactory bulb LFPs from behaving mice (Fig. 4), a total of 2 male ICR mice (3–4 months old) with preoperative weights of 45–50 g was used in this study. The detailed surgical procedures have been described elsewhere[8,9]). Briefly, mice were anesthetized with 1–2% isoflurane gas in air, and an incision (~1 cm) was made on each side of the upper chest. Then, 2 ECG electrodes (AS633, Cooner Wire Company) were sutured to the tissue underneath the skin of the upper chest. Circular craniotomies (1 mm in diameter) were made and stainless steel screws were implanted at the following coordinates: 5.0 mm anterior and 0.5 mm unilateral to bregma for the olfactory bulb (as an indicator of respiration); 6.5 mm posterior and 1.5 mm bilateral to bregma for the cerebellum (as ground). After all surgical procedures were complete, anesthetic administration was stopped, and the mice were allowed to awaken from the anesthesia spontaneously. For postoperative recovery, each mouse was housed individually in a cage for more than one week until its body weight returned to the preoperative level.

For *in vivo* whole-cell recordings (Fig. 5), 28- to 40-day-old male ICR mice (Japan SLC, Shizuoka, Japan) were used as previously described.[10,11] Briefly, the mice were anesthetized with urethane (2.25 g/kg, intraperitoneal [i.p.]). The skin was subsequently removed from the head, and the animal was implanted with a metal head-holding plate. A craniotomy (2.5 × 2.0 mm^2) was then performed, centered at 2.0 mm posterior to the bregma and 2.5 mm ventrolateral to the sagittal suture, and the neocortex above the hippocampus was carefully aspirated.[12] The exposed hippocampal window was covered with 1.7% agar at a thickness of 1.5 mm.

2.3. Behavioral task

For chronic recordings (Fig. 4), mice were allowed to explore an elevated plus maze, which was made of acrylonitrile butadiene styrene resin and consisted of a central square (7.6 × 7.6 cm) and four arms (28 cm long × 7.6 cm wide, two open arms with no railing and two closed arms enclosed by vertical walls 15 cm in height). The maze was elevated 30 cm from the floor. In each recording session, a mouse was placed in the middle of the central square, facing one of the open arms, and explored the maze apparatus for 5 min. The floor of the apparatus was cleaned with water and 70% ethanol after every exploration period.

2.4. Data acquisition

Simultaneous recordings of ECG signals, abdominal movement signals and olfactory bulb LFPs were made at a sampling frequency of 2 kHz using a CerePlex Direct recording system (Blackrock Microsystems, Salt Lake City, UT, USA). The physical abdominal movement was first converted into a change in electrical potentials through an isotonic transducer. The signal was then transmitted to the CerePlex system. These three bio-signals were recorded for 5 min.

For chronic recordings, the animal's behavior in the maze was monitored at a frame rate of 60 Hz using a top-view video camera. The frame rate of the video was down-sampled to 3 Hz, and the instantaneous speed of the animal in each frame was calculated from the distance traveled within a frame (~333 ms). The ECG signals and the olfactory bulb LFPs were acquired using a CerePlex Direct recording system.

Whole-cell recordings were made from pyramidal neurons in the CA1 *stratum pyramidale* using borosilicate glass electrodes (4–7 MΩ). Pyramidal cells were identified by their regular spiking properties and by *post hoc* histological analysis.[12] For current-clamp recordings, the intra-pipette solution contained the following solutes (in mM): 120 potassium gluconate, 10 KCl, 10 HEPES, 10 creatine phosphate, 4 MgATP, 0.3 Na_2GTP, 0.2 EGTA (pH 7.3), and 0.2% biocytin. Cells were discarded when the series resistance exceeded 75 MΩ or the mean resting potential exceeded −55 mV. Moreover, recordings were rejected when the resting potential increased by more than 8 mV from its value at the onset of the recording. ECG signals were simultaneously acquired as described above. The neuronal and cardiac signals were amplified by a MultiClamp 700 B (Molecular Devices, Union City, CA, USA) and a DAM80 (World Precision Instruments, Sarasota, FL, USA), respectively. All the signals were digitized at 20 kHz by a Digidata 1440A (Molecular Devices) and analyzed with pCLAMP 10.3 (Molecular Devices).

All signals were acquired at a room temperature.

2.5. Drugs

Acetazolamide (0.4 mg/kg, i. v., MP Biomedicals, Solon, OH, USA)[13] and diazepam (0.2 mg/kg, i. v., Wako, Osaka, Japan)[14] were

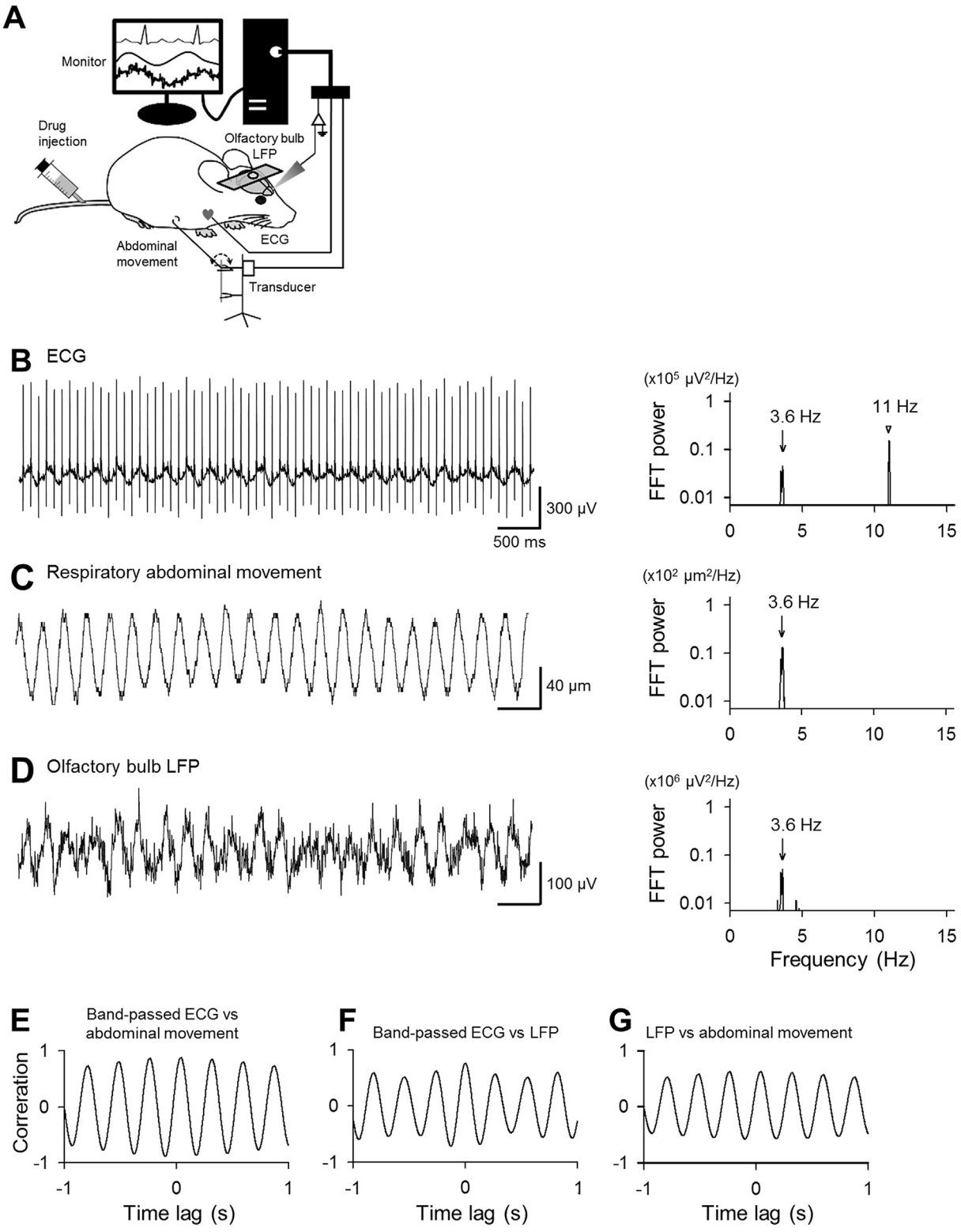

Fig. 1. Simultaneous recordings of ECGs, respiratory abdominal movement, and olfactory bulb LFPs from an anesthetized mouse. *A*, A diagram of the experimental setup. *B*, *Left*: A representative raw ECG trace. *Right*: The fast Fourier transform (FFT) power spectral density of the ECG trace, in which two peaks are indicated by the arrows. *C*, A representative raw trace of abdominal movement (*Left*) and its FFT spectrum (*Right*). Note that the trough-to-peak portion (*i.e.*, ascending phase) and the peak-to-trough portion (*i.e.*, descending phase) in the abdominal movement trace correspond to inhalation and exhalation, respectively. *D*, A representative raw trace of the olfactory bulb LFPs (*Left*) and the FFT spectrum of the trace (*Right*). The traces shown in *B*–*D* were simultaneously obtained from the same mouse. *E*–*G*, Cross-correlations between ECG signal and abdominal movement (*E*), between ECG signal and LFPs (*F*), and between LFPs and abdominal movement (*G*). The ECG signals were band-passed between 1.5 and 5.5 Hz to remove heartrate-relevant signals.

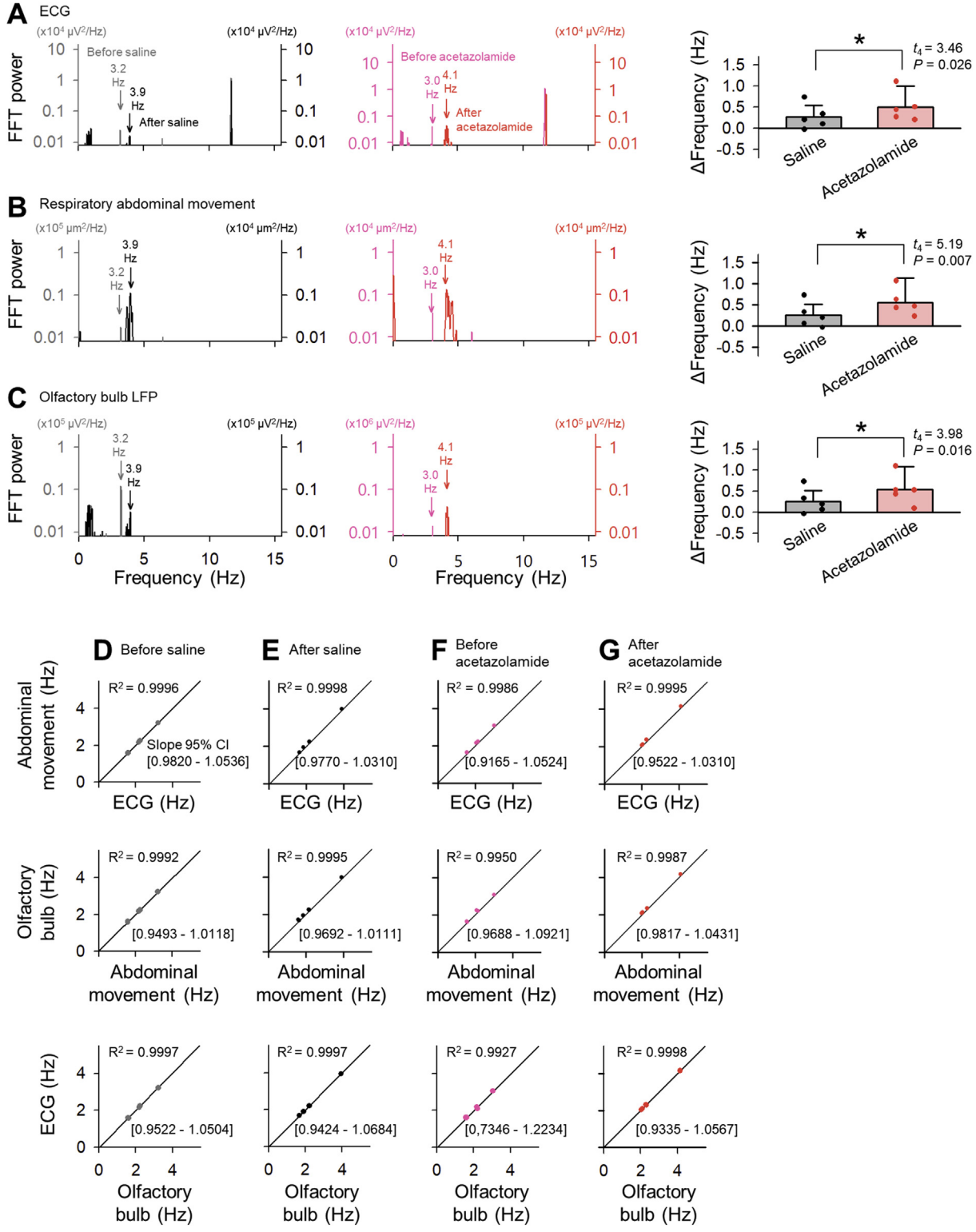

Fig. 2. Effects of acetazolamide on the ECG-derived respiratory component. *A*, The *left* and *middle* panels show the FFT power spectral densities of the ECGs before (*light color*) and after (*dark color*) intravenous injection of saline and 0.4 mg/kg acetazolamide, respectively. The data are summarized in the bar graph on the *right*, representing the mean ± SD changes in the peak frequencies (Δfrequency) of the low-frequency ECG components after administration of saline and acetazolamide. The *P* and *t* values were obtained by paired *t*-tests, with $n = 5$ mice. *B, C*, The same as *A*, but for respiratory abdominal movement (*B*) and olfactory bulb LFPs (*C*). *D*–*G*, Linear regressions between all possible pairs among the three respiratory rates recorded by ECGs, abdominal movement, and olfactory bulb LFPs were performed before (*D*, *F*) and after (*E*, *G*) injection of saline (*D*, *E*) and acetazolamide (*F*, *G*). The coefficients of determination (R^2) are shown above the regression lines, and the 95% confidence intervals of the slopes of the regression lines are shown under the lines. Note that all 95% confidence intervals include 1. $n = 5$ mice each.

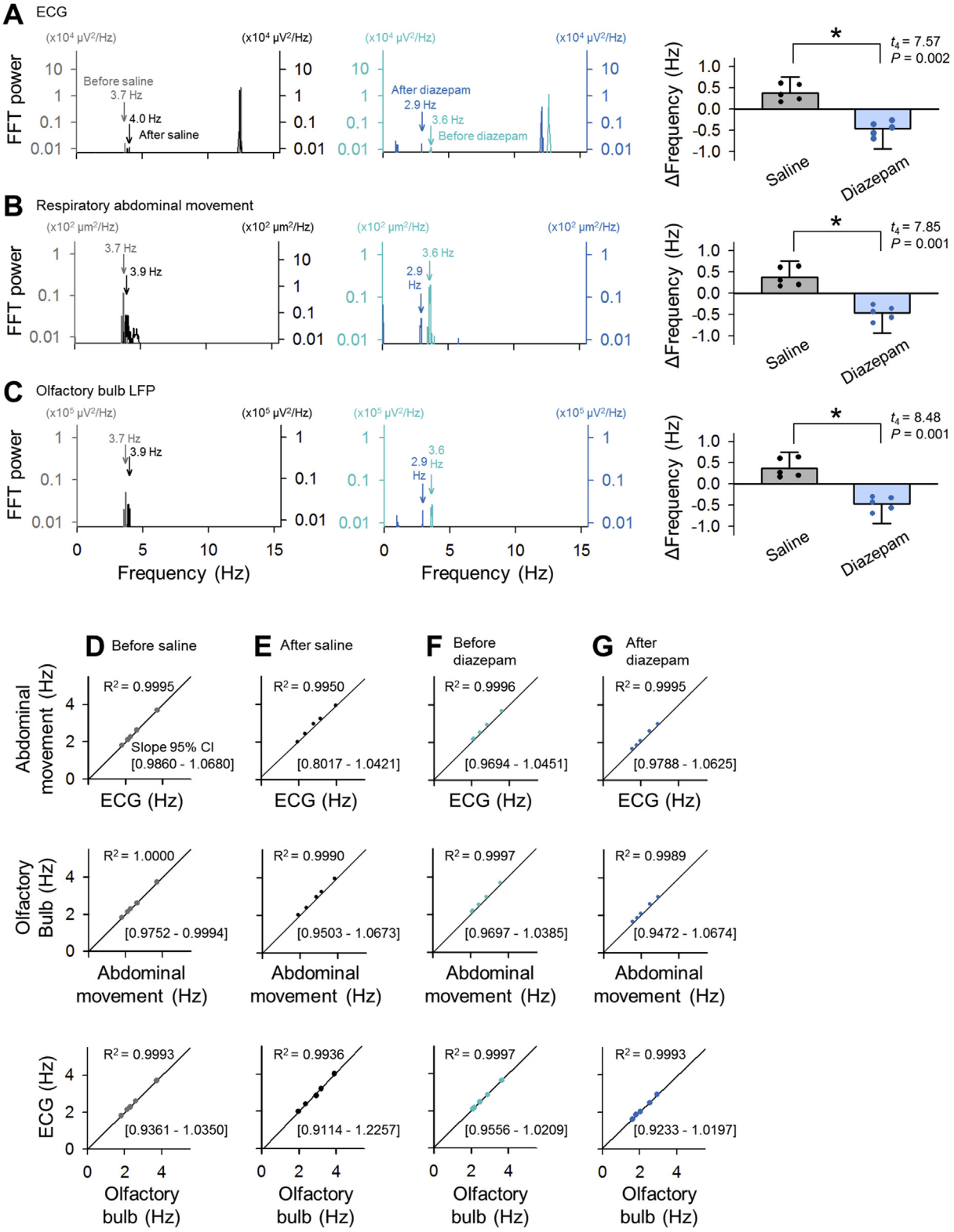

Fig. 3. Effects of diazepam on a respiratory component of ECGs. The same as Fig. 2, but for 0.2 mg/kg diazepam. *A*–*C*, The *left* and *middle* panels show the FFT power spectral densities of the ECGs (*A*), the respiratory abdominal movement (*B*) and the olfactory bulb LFPs (*C*) before (*light color*) and after (*dark color*) tail-vein injection of saline and diazepam, respectively. The data are summarized in the bar graphs on the *right*, representing the mean ± SD changes in the peak frequencies (Δfrequency) of the low-frequency ECG components after administration of saline and diazepam. The *P* and *t* values were obtained by paired *t*-tests, with $n = 5$ mice. *D*–*G*, Linear regressions between all possible pairs among the three respiratory rates recorded by ECGs, abdominal movement, and olfactory bulb LFPs were performed before (*D*, *F*) and after (*E*, *G*) injection of saline (*D*, *E*) and diazepam (*F*, *G*). The coefficients of determination (R^2) are shown above the regression lines, and the 95% confidence intervals of the slopes of the regression lines are shown under the lines. $n = 5$ mice each.

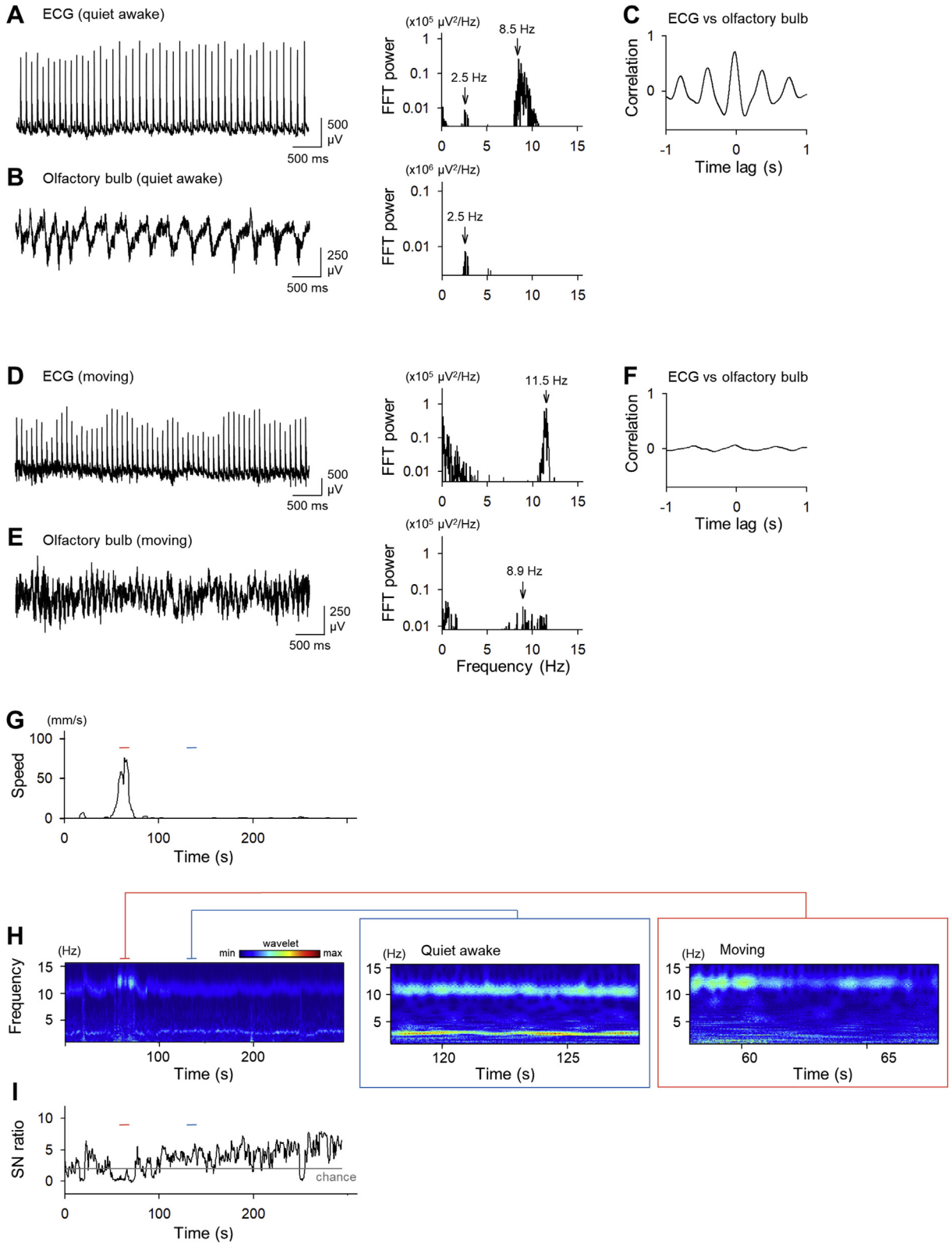

Fig. 4. ECG recordings from awake mice. *A*, *B*, Representative simultaneously recorded traces (*left*) of ECG signals (*A*) and olfactory bulb LFPs (*B*) and their FFT power spectral densities (*right*) during quiet awake periods in an unanesthetized mouse. *C*, The cross-correlogram of the band-passed (1.5–5.5 Hz) ECGs *versus* the olfactory bulb LFPs during quiet, immobile periods in an unanesthetized mouse. *D*–*F*, The same as *A*–*C*, but for the moving period. *G*–*I*, The running speed of the mouse (*G*), pseudo-colored wavelet matrices (*H*), and the SN ratio (*I*) during a representative recording session. The SN ratio represents the detectability of the FFT peak in the 1.5–5.5 Hz range against the background noise and exceeded its chance level when the running speed dropped into zero. In panel *H*, the matrices during the quiet awake and moving periods are expanded in the insets on the *right*. The data shown in *G*–*I* were obtained simultaneously.

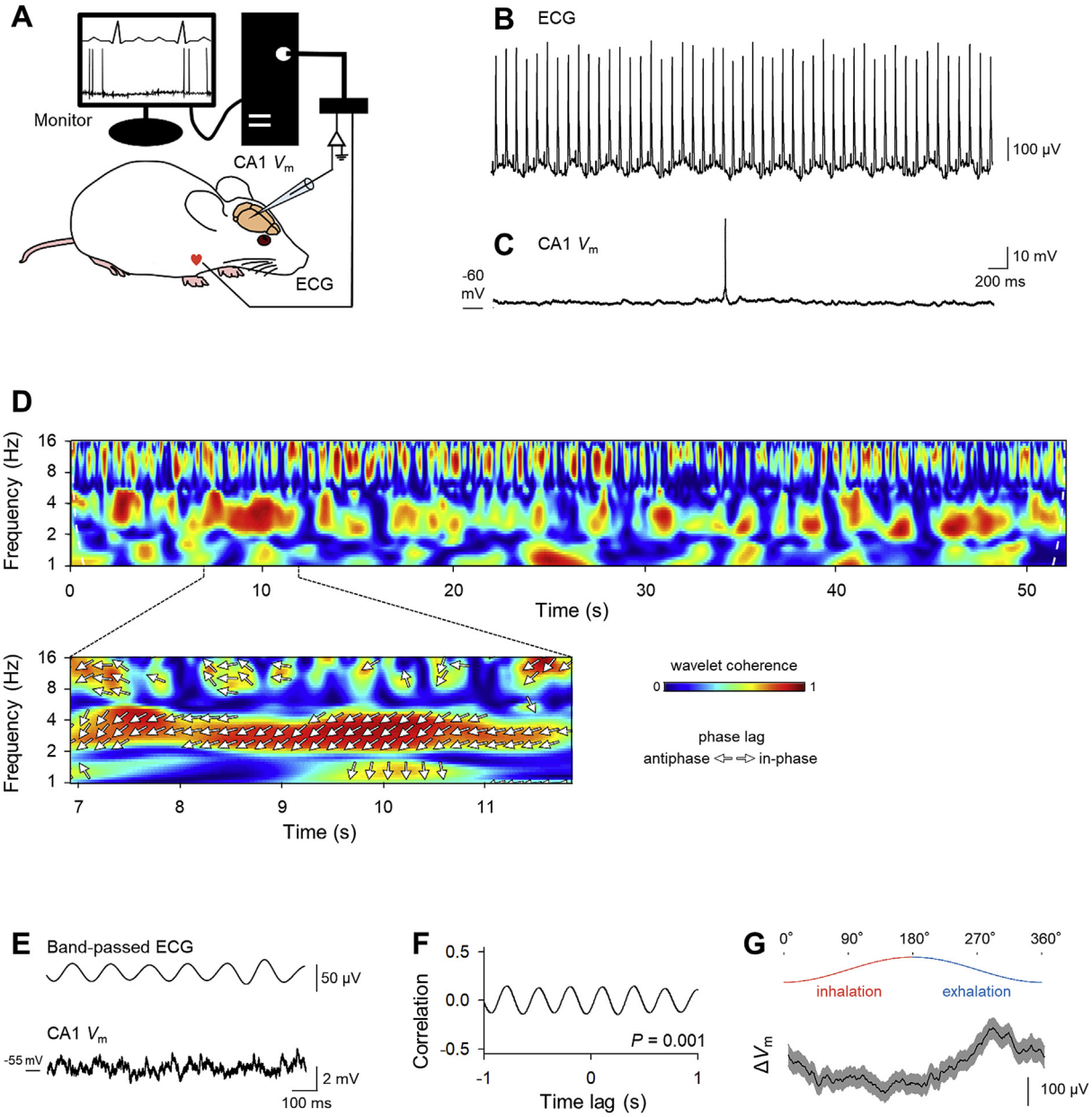

Fig. 5. Simultaneous recordings of ECGs and membrane potentials of single hippocampal CA1 neurons. *A*, An experimental setup. *B*, *C*, Simultaneously recorded ECGs (*B*) and V_m of a whole-cell current-clamped CA1 neuron (*C*) in an anesthetized mouse. *D*, Wavelet coherence between ECGs and V_m as a function of time. The cones of influence are indicated by the *white* dashed line at the beginning and end of the time axis. Part of the wavelet coherence graph is expanded in the *bottom* inset, in which the coherence at approximately 3 Hz continuously exceeded 0.5. The relative coherence lags (*i.e.*, phases indicated by *arrows*) between ECGs and V_m were calculated using the wavelet cross-spectra. Note that the coherence lags at approximately 3 Hz (*i.e.*, respiratory rates) remained nearly consistent over time. *E*, *F*, Representative traces of the band-passed ECGs and V_m of a respiratory-correlated CA1 neuron (*E*) and their cross-correlation (*F*). *G*, The average V_m change during a single respiratory cycle. The ascending (0°–180°, *red*) and descending (180°–360°, *blue*) phases of the cycle indicate inhalation and exhalation, respectively. The mean ΔV_m trace (*black*) is superimposed onto a range of ±1 SEM (*gray*) for 369 cycles from 4 neurons.

injected to increase and decrease the respiratory rate, respectively. Each drug was injected into the tail vein 100 s after the beginning of the recording. As a control, saline was injected before the two drugs.

2.6. Data analysis

All data analyses were carried out using ImageJ and custom-made algorithms written in MATLAB (MathWorks, Natick, MA, USA).

We assumed that lateral abdominal movement and olfactory bulb LFPs were indicators of respiration and confirmed whether the low-frequency components of the ECGs corresponded to the respiratory rate by analyzing frequency spectra obtained by the fast Fourier transform (FFT). To evaluate the time lag between each pair of those three signals, we first band-passed the original ECG signals at 1.5–5.5 Hz, a frequency range of respiration, and then calculated the cross-correlation in each pair.

To estimate how our arithmetic isolation between respiratory and heartbeat rhythms is affected by the murine morphology, we calculated the integral ratio of the ECG power spectral density between 1.5 and 5.5 Hz (respiratory power) to that between 7 and 15 Hz (cardiac power), regarded the body weight as a measure of its morphology, and then compared the ratio with the weight.

To investigate respiratory sinus arrhythmia, we applied spline interpolation to R–R intervals (RRIs) and filtered them at band

frequencies between 1.5 and 5.5 Hz. These band-passed RRIs were defined as RRI signals. We then calculated the cross-correlation function between the RRI signals and ECG-derived respiratory signals.

In the pharmacological experiments, we compared the peak frequency in the power spectral density from 30-s-long periods before and after drug injection.

In the experiments with waking mice, we analyzed running speed using ImageJ and compared the quiet awake state (*i.e.*, approximately 0 mm/s) with the moving state (*i.e.*, over 0 mm/s). To quantify the extent of isolation of respiratory signals from cardiac ones, we scanned the original ECGs with a sliding 5-s window. We then calculated the signal-to-noise (SN) ratio for each window according to the following definition:

$$\text{SN ratio} = \frac{M - \mu}{\sigma},$$

where M is the peak value in the power spectral density (1.5–5.5 Hz) of the focused ± 2.5-s time window, and the values μ and σ are the mean and SD, respectively, of the power spectral density (0–15 Hz) within the same window. To characterize the ECG signals in a time-frequency domain, we further convoluted the ECG signals with a Morlet wavelet family.

To investigate the relationship between ECGs and the membrane potentials (V_m) of CA1 neurons, we first calculated the wavelet coherence[15] between ECGs and CA1 V_m. We next determined whether the CA1 V_m was correlated with respiration. The ECGs were band-passed at 1.5–5.5 Hz; thereby, the respiratory rhythms were derived from the ECGs. Then, we computed the cross-correlation function between the CA1 V_m and respiratory oscillations and compared the maximum correlation coefficient with the chance level. To estimate the chance level, we divided the original membrane potential traces, in which action potentials were truncated, into 100-ms segments. We then combined them in a randomly shuffled order and generated a surrogate. We repeated this randomization and obtained 10,000 surrogates, after which we estimated the P value. Furthermore, we calculated the respiratory phase from the band-passed ECG signals. We defined the trough as 0° and 360°, and the peak as 180°. The trough-to-peak and peak-to-trough periods corresponded to inhalation and exhalation, respectively. We investigated the relationship of the respiratory phase and the relative membrane potentials to the average membrane potentials during each respiratory cycle.

All data were represented as the means ± SD unless otherwise specified. The null hypothesis was rejected at the $P < 0.05$ level unless otherwise specified.

3. Results

We observed low-frequency (*i.e.*, approximately 3- to 4-Hz) fluctuations in the baseline of ECG signals recorded from urethane-anesthetized mice. To confirm that the low-frequency component reflects the respiratory rhythm, we recorded physical movement of the side of abdomen and LFPs in the olfactory bulb simultaneously with ECGs (Fig. 1A). Time-series analyses using the fast Fourier transform (FFT) revealed that the ECGs exhibited two peaks in their power spectral density (Fig. 1B), whereas the abdominal movement signal and the olfactory bulb LFPs each exhibited one peak, which corresponded to the lower-frequency peak in the ECGs (Fig. 1C, D). Because it is possible that these respiratory signals depend on murine morphology, we compared the ratio of the respiratory power to cardiac power with the mouse body weight (see Materials and methods); however, these correlations were not significantly different from zero ($P = 0.92$, $t_8 = 0.25$, Student's t-test of a correlation coefficient *vs* 0). To characterize the temporal features of these three bio-signals (*i.e.*, three pairs), we computed the cross-correlations between them (Fig. 1E–G). All three cross-correlations fluctuated periodically at frequencies of 3–4 Hz and peaked at approximately 0 s (band-passed ECG *vs* abdominal movement: 29 ± 109 ms; band-passed ECG *vs* LFP: −19 ± 34 ms; LFP *vs* abdominal movement: −18 ± 102 ms; mean ± SD of 10 mice). Therefore, we concluded that the lower-frequency component of the ECG signal arose from respiration.

The heartbeats are modulated by the respiratory cycles of inhalation and exhalation in humans, a phenomenon that is known as respiratory sinus arrhythmia.[16,17] We examined whether the respiratory sinus arrhythmia occur in mice in our experimental conditions. We calculated the cross-correlation function between RRI signals and respiratory signals (see Materials and methods) and estimated the time lags of these two signals. As the lungs expand, the respiratory signals become relatively positive, whereas the RRI signals become relatively negative as RRIs are shortened. Thus, the resultant antiphase signals are expected to yield a negative peak at time zero in the cross-correlation function.[18] However, the actual results were partially consistent across animals; we observed such a negative peak in some mice, but did not in the others (*data not shown*).

To confirm that the changes in respiratory rates are faithfully reflected in the low-frequency component of ECGs in real time, we conducted pharmacological manipulations of the respiratory rhythm. Mice were intravenously treated with saline or 0.4 mg/kg acetazolamide, which is known to increase respiratory rates.[13] We computed the FFT spectral densities of three bio-signals and measured their peak frequencies between 1.5 and 5.5 Hz as the respiratory rates (Fig. 2A–C). Twenty seconds after the treatment, the respiratory rates of acetazolamide-treated mice as measured through ECGs, abdominal movement, and olfactory bulb LFPs were significantly higher than those of saline-treated mice (ECG: 0.27 ± 0.29 Hz (saline) *vs.* 0.50 ± 0.36 Hz (acetazolamide), $P = 0.026$, $t_4 = 3.46$, paired t-test; abdominal movement: 0.26 ± 0.30 Hz *vs.* 0.57 ± 0.31 Hz, $P = 0.007$, $t_4 = 5.19$; olfactory bulb LFP: 0.26 ± 0.30 Hz *vs.* 0.54 ± 0.36 Hz, $P = 0.016$, $t_4 = 3.98$; $n = 5$ mice). We also plotted the respiratory rates before and after saline or acetazolamide injection in a two-dimensional coordinate system and determined the regression lines using the least-squares method (Fig. 2D–G). The regression lines were not significantly different from the diagonal line $y = x$ because the 95% confidence intervals of their slopes included 1.

We next treated mice with saline or 0.2 mg/kg diazepam, which is known to reduce the respiratory rate,[14] and conducted the same analyses for three bio-signals (Fig. 3A–C). The respiratory rates of diazepam-injected mice were significantly lower than those of saline-injected mice (ECG: 0.38 ± 0.20 Hz (saline) *vs.* −0.47 ± 0.17 Hz (diazepam), $P = 0.002$, $t_4 = 7.57$, paired t-test; abdominal movement: 0.38 ± 0.22 Hz *vs.* −0.47 ± 0.17 Hz, $P = 0.001$, $t_4 = 7.8$; olfactory bulb LFP: 0.38 ± 0.23 Hz *vs* −0.47 ± 0.17 Hz, $P = 0.001$, $t_4 = 8.48$; $n = 5$ mice). Two-dimensional plots of the respiratory rates also demonstrated that the regression lines were statistically identical to $y = x$ (Fig. 3D–G). Therefore, the respiratory rates measured by the three bio-signals were tightly linked and fluctuated in response to pharmacological manipulations.

We next recorded ECG signals and olfactory bulb LFPs from mice that were freely exploring an elevated plus maze to examine whether the respiratory rhythms can be extracted from the ECGs of unanesthetized animals. We analyzed the bio-signals during quiet awake and moving periods separately. During quiet awake states, the low-frequency oscillations of the ECGs and the olfactory bulb LFPs peaked at the same frequency in the FFT power spectral densities (Fig. 4A, B) and exhibited peak cross-correlation at time

0 (Fig. 4C). During moving states, the ECG waveform appeared turbulent and did not clearly exhibit a single peak in its power spectral density (Fig. 4D). The olfactory bulb LFPs exhibited higher-frequency oscillations, indicating increased respiratory rates (Fig. 4E). In contrast to the quiet awake state (Fig. 4C), the cross-correlation exhibited no apparent peak at time 0 in the behaving state (Fig. 4F), which suggests the low-frequency component of ECGs in behaving mice is no longer correlated with olfactory LFPs. Therefore, we analyzed the relationship between running speed and the performance for frequency-based isolation of respiratory signals from ECGs. We first computed the average running speed for every five-second window (Fig. 4G). We then performed the wavelet transform of ECGs during the entire recording time (Fig. 4H). Prominent respiratory signals (*i.e.*, approximately 3 Hz) were observed when the running speed was close to 0 mm/s (*i.e.*, in quiet awake states), whereas the respiratory signals became vague while the mouse was actively behaving. To quantify these data, we computed the SN ratios of the low-frequency component of the ECGs as a function of time (see Materials and methods). The SN ratios were high only while the running speed was approximately 0 mm/s, and they became lower than the chance level while the mice moved (Fig. 4I).

A previous study demonstrated that LFP oscillations in the hippocampi of anesthetized rodents are associated with respiratory rhythms.[19] Thus, using the whole-cell current-clamp technique, we recorded the membrane potentials (V_m) of hippocampal CA1 neurons together with the ECGs of anesthetized mice (Fig. 5A–C). We found that the wavelet coherences[15] between ECGs and CA1 V_m at approximately 3 Hz (respiration) and 10 Hz (heartbeat) were intermittently elevated. During the high-coherence states, the phase lags at 3 Hz were almost constant over time, whereas the lags at 10 Hz varied (arrows in the inset of Fig. 5D), suggesting that neuronal V_m values were more coherent with respiratory rhythms rather than cardiac rhythms. We thus computed the cross-correlations between the band-passed ECGs and CA1 V_m and found that 4 out of the 8 tested neurons exhibited correlations significantly higher than the chance level (Fig. 5E, F). Phase analyses revealed that in these respiration-correlated neurons, V_m fluctuated along a respiratory cycle; that is, V_m hyperpolarized during inhalation and depolarized during exhalation (Fig. 5G).

4. Discussion

In the present study, we developed a reliable method to monitor intact respiratory signals of mice through a single precordial electrode and simple mathematical algorithm to isolate respiratory signals from ECGs. We demonstrated the successful isolation of respiratory rates from ECG baseline oscillations in anesthetized and waking mice, which was confirmed using physiological recording of multiple bio-signals and pharmacological manipulation. The ECG baseline oscillated with high amplitudes so that FFT, a computationally costless algorithm, could stably isolate the respiratory rhythms. This isolation process is simple and rapid, and thus it will be implementable for simultaneous recordings of multiple bio-signals as well as real-time feedback manipulations of biological activity in various animal experiments.

We assume that the mechanism for the ECG-derived respiratory monitoring in mice is the same as that in humans. In humans, it is widely known that respiratory components are superimposed onto the ECG signal, and various techniques have been proposed to isolate it.[6,7,16,20] They include two methods. One utilizes respiratory sinus arrhythmia, which is caused by heartbeats modulated by inhalation and exhalation.[7,16] The other utilizes the fluctuations in R-wave amplitudes, which are caused by respiration-induced changes in the impedance in the thoracic cavity.[6,7,20] We applied the latter mechanism to small animals.

In contrast to previous studies,[7,16,17] we could not stably observe respiratory sinus arrhythmia. We attribute one possible reason to anesthesia by urethane. Urethane anesthesia tends to induce releases of noradrenaline and adrenaline, leading to sympathetic dominance over parasympathetic modulations.[21] Because the parasympathetic nervous activity is important for respiratory sinus arrhythmia,[22] we might have failed to observe the respiratory sinus arrhythmia.

We could not isolate the respiratory signal from the ECGs during active exploration periods. We have identified two possible reasons: 1) large muscular electrical signals may have masked the low-frequency component of the ECGs, or 2) respiratory components may have fallen within the heartbeat components because physical exercise increased the respiratory rates.

Some previous methods of monitoring respiration have utilized sensors in the nasal cavity that stimulated nasal receptors,[3–5] altering the patterns of respiration. In contrast to those approaches, our method does not obstruct the nasal airway. Moreover, it does not disturb other respiratory organs, including the trachea and the lungs. To achieve this method efficiently, we carefully chose the pectoral muscle, rather than other body parts, because we found that ECG recorded from the pectoral muscle most clearly reflected respiratory signals. As a result, our method enables us to easily and accurately acquire respiratory signals and is used in combination with monitoring other bio-activities such as neural activity to analyze the across–modality correlations, which may provide us with more precise prediction of adverse effects of drugs as well as evaluation of drug efficacy. Further, our technique is applicable to pharmacokinetic analysis, which allows for better drug development in the future. For example, stress is associated with respiration[23] and is one of the major causes of psychiatric disorders.[24] In addition, self-regulation of respiration is suggested as a treatment strategy for psychiatric disorders.[25] However, it is not fully understood how respiration and neural activity are modulated by stress, how the modulation causes psychiatric disorders, and how the disorders are rescued pharmacologically. With this respect, our novel technique serves as a step to discover the respiratory–neural interaction in psychiatric disorders, driving researches on drugs that have clinical effects on these disorders via modulation of respiration. Thus, our present technique may benefit drug discovery for the central nervous system, which is still challenging and developing.

In rodents, it is controversial whether neuronal activity is associated with respiration.[26–30] These discrepancies are partially reconciled by a recent study;[19] however, this study used cannulae in the nasal cavity to measure respiratory rhythms and could not exclude the possibility that respiration was unnaturally assessed.[19] Such invasive measurement of respiration causes impairment of olfactory epithelium and may alter LFPs in the hippocampus via the olfactory bulb-to-entorhinal cortex-to-hippocampus pathway, making it difficult to precisely relate respiration and information processing in the brain. Thus, a less invasive method is required for monitoring the respiratory rhythms. Our simple and reliable technique can be combined with various pharmacological and neurophysiological experiments. In this study, for example, we simultaneously monitored the respiration rhythm and V_m of single hippocampal neurons using *in vivo* whole-cell recordings. As a result, we found that in some neurons, the subthreshold V_m fluctuated in conjunction with respiration rather than heartbeat. Therefore, we speculate that respiration can modulate the V_m behaviors of hippocampal neurons. To the best of our knowledge, no experimental or clinical studies have reported such intracellular modulations. However, we do not exclude the possibility that the

respiration-associated V_m oscillations were merely due to respiration-induced physical movement of the brain.[31] Further experiments are required to investigate whether CA1 neurons receive respiration-relevant synaptic inputs and thereby generate oscillatory V_m dynamics. For example, simultaneous *in vivo* whole-cell recordings of multiple CA1 neurons, together with an ECG recording, will reveal the dependence of the V_m oscillations on respiration.

Previous studies have suggested that respiratory rhythms are an important influence on information processing in the brain.[32] Moreover, it has recently been suggested that respiration-related olfactory oscillations drive extracellular oscillations in the whisker barrel cortex of waking animals[27] and that respiration entrains hippocampal LFP oscillations.[28,29] Our recording methods can further be combined with extracellular or intracellular recordings from the limbic system, including the hippocampus, entorhinal cortex and amygdala, and will provide a simple avenue to approach the functional relevance of respiration to information processing in memory and emotion.

Conflict of interest

The authors have no conflict of interest to disclose with respect to this research.

Acknowledgments

This work was supported by Grants-in-Aid for Scientific Research (26250003; 25119004) and by the Human Frontier Science Program (RGP0019/2016). This work was conducted partly as a program at the International Research Center for Neurointelligence (WPI-IRCN) of The University of Tokyo Institutes for Advanced Study at The University of Tokyo.

References

1. Fisch C. Evolution of the clinical electrocardiogram. *J Am Coll Cardiol*. 1989;14:1127–1138.
2. Matsukura S, Nakamura Y, Hoshiai K, et al. Effects of moxifloxacin on the proarrhythmic surrogate markers in healthy Filipino subjects: exposure-response modeling using ECG data of thorough QT/QTc study. *J Pharmacol Sci*. 2018;136:234–241.
3. Lenz G, Heipertz W, Epple E. Capnometry for continuous postoperative monitoring of nonintubated, spontaneously breathing patients. *J Clin Monit*. 1991;7:245–248.
4. Marks MK, South M, Carter BG. Measurement of respiratory rate and timing using a nasal thermocouple. *J Clin Monit*. 1995;11:159–164.
5. Perez W, Tobin MJ. Separation of factors responsible for change in breathing pattern induced by instrumentation. *J Appl Physiol*. 1985;59:1515–1520.
6. Penzel T, McNames J, Murray A, de Chazal P, Moody G, Raymond B. Systematic comparison of different algorithms for apnoea detection based on electrocardiogram recordings. *Med Biol Eng Comput*. 2002;40:402–407.
7. Boyle J, Bidargaddi N, Sarela A, Karunanithi M. Automatic detection of respiration rate from ambulatory single-lead ECG. *IEEE Trans Inf Technol Biomed*. 2009;13:890–896.
8. Okada S, Igata H, Sakaguchi T, Sasaki T, Ikegaya Y. A new device for the simultaneous recording of cerebral, cardiac, and muscular electrical activity in freely moving rodents. *J Pharmacol Sci*. 2016;132:105–108.
9. Sasaki T, Nishimura Y, Ikegaya Y. Simultaneous recordings of central and peripheral bioelectrical signals in a freely moving rodent. *Biol Pharm Bull*. 2017;40:711–715.
10. Funayama K, Minamisawa G, Matsumoto N, et al. Neocortical rebound depolarization enhances visual perception. *PLoS Biol*. 2015;13, e1002231.
11. Ishikawa D, Matsumoto N, Sakaguchi T, Matsuki N, Ikegaya Y. Operant conditioning of synaptic and spiking activity patterns in single hippocampal neurons. *J Neurosci*. 2014;34:5044–5053.
12. Matsumoto N, Okamoto K, Takagi Y, Ikegaya Y. 3-Hz subthreshold oscillations of CA2 neurons in vivo. *Hippocampus*. 2016;26:1570–1578.
13. Hackett PH, Roach RC, Harrison GL, Schoene RB, Mills Jr WJ. Respiratory stimulants and sleep periodic breathing at high altitude. Almitrine versus acetazolamide. *Am Rev Respir Dis*. 1987;135:896–898.
14. Bonora M, St John WM, Bledsoe TA. Differential elevation by protriptyline and depression by diazepam of upper airway respiratory motor activity. *Am Rev Respir Dis*. 1985;131:41–45.
15. Grinsted A, Moore JC, Jevrejeva S. Application of the cross wavelet transform and wavelet coherence to geophysical time series. *Nonlin Process Geophys*. 2004;11:561–566.
16. Schafer A, Kratky KW. Estimation of breathing rate from respiratory sinus arrhythmia: comparison of various methods. *Ann Biomed Eng*. 2008;36:476–485.
17. Ludwig C. Beiträge zur kenntniss des einflusses der respirationsbewegungen auf den blutlauf im aortensysteme. *Arch Anat Physiol*. 1847;13:242–302.
18. Yasuma F, Hayano J. Respiratory sinus arrhythmia: why does the heartbeat synchronize with respiratory rhythm? *Chest*. 2004;125:683–690.
19. Lockmann AL, Laplagne DA, Leao RN, Tort AB. A respiration-coupled rhythm in the rat hippocampus independent of theta and slow oscillations. *J Neurosci*. 2016;36:5338–5352.
20. Moody GB, Mark RG, Zoccola A, Mantero S. Derivation of respiratory signals from multi-lead ECGs. *Comput Cardiol*. 1985;13:113–116.
21. Armstrong JM, Lefevre-Borg F, Scatton B, Cavero I. Urethane inhibits cardiovascular responses mediated by the stimulation of alpha-2 adrenoceptors in the rat. *J Pharmacol Exp Ther*. 1982;223:524–535.
22. Katona PG, Jih F. Respiratory sinus arrhythmia: noninvasive measure of parasympathetic cardiac control. *J Appl Physiol*. 1975;39:801–805.
23. Grossman P. Respiration, stress, and cardiovascular function. *Psychophysiology*. 1983;20:284–300.
24. Iñiguez SD, Riggs LM, Nieto SJ, et al. Social defeat stress induces a depression-like phenotype in adolescent male c57BL/6 mice. *Stress*. 2014;17:247–255.
25. Jerath R, Crawford MW, Barnes VA, Harden K. Self-regulation of breathing as a primary treatment for anxiety. *Appl Psychophysiol Biofeedback*. 2015;40:107–115.
26. Nguyen Chi V, Muller C, Wolfenstetter T, et al. Hippocampal respiration-driven rhythm distinct from theta oscillations in awake mice. *J Neurosci*. 2016;36:162–177.
27. Ito J, Roy S, Liu Y, et al. Whisker barrel cortex delta oscillations and gamma power in the awake mouse are linked to respiration. *Nat Commun*. 2014;5:3572.
28. Yanovsky Y, Ciatipis M, Draguhn A, Tort AB, Brankack J. Slow oscillations in the mouse hippocampus entrained by nasal respiration. *J Neurosci*. 2014;34:5949–5964.
29. Liu Y, McAfee SS, Heck DH. Hippocampal sharp-wave ripples in awake mice are entrained by respiration. *Sci Rep*. 2017;7:8950.
30. Viczko J, Sharma AV, Pagliardini S, Wolansky T, Dickson CT. Lack of respiratory coupling with neocortical and hippocampal slow oscillations. *J Neurosci*. 2014;34:3937–3946.
31. Matsumoto N, Takahara Y, Matsuki N, Ikegaya Y. Thoracotomy reduces intrinsic brain movement caused by heartbeat and respiration: a simple method to prevent motion artifact for in vivo experiments. *Neurosci Res*. 2011;71:188–191.
32. Fontanini A, Bower JM. Slow-waves in the olfactory system: an olfactory perspective on cortical rhythms. *Trends Neurosci*. 2006;29:429–437.